Failure mechanisms and reliability of the Al-chip-metallization during power cycling

Camille Durand, Daniel Coutellier, Hakim Naceur, Markus Klingler

Failure mechanisms and reliability of the Al-chip-metallization during power cycling

C. DURAND[abc], M. KLINGLER[a], D. COUTELLIER[bc], H. NACEUR[bc]

a.Robert Bosch GmbH, Automotive Electronics, Markwiesenstr. 46, 72770 Reutlingen, Germany
b.LAMIH UMR CNRS 8201, University of Valenciennes, Le Mont Houy, 59313 Valenciennes Cedex 9, France
c.ENSIAME, University of Valenciennes, Le Mont Houy, 59313 Valenciennes Cedex 9, France
e-mail: camille.durand@univ-valenciennes.fr

Résumé :

Cet article étudie les mécanismes de rupture et la fiabilité de la couche de métallisation d'une puce électronique d'un nouveau module de puissance, remplaçant les fils de connexion par un clip en cuivre. A la fois des tests de cycles actifs de puissance et des simulations thermomécaniques par éléments finis ont été réalisés. Cette étude utilise les simulations numériques pour analyser en détail les déformations plastiques et la propagation de fissures dans la métallisation de la puce sous différents cycles actifs de puissance. Les modèles de durée de vie sont ensuite déduits en corrélant la durée de vie des modules obtenue par expérimentation avec les déformations plastiques et les critères de propagations de fissures calculés correspondants.

Abstract:

This paper studies the failure mechanisms and the reliability of the chip-metallization of a new power module using a copper clip soldered on the top side of the chip, instead of aluminum wire bonds. Both power cycling tests and thermo-mechanical Finite Elements simulations are performed. This study takes advantages of the numerical simulations to analyze in details plastic strains and crack growth in the chip-metallization under different Active Power Cycling conditions. Lifetime models are then deduced by correlating the experimentally obtained lifetime with the corresponding calculated plastic strains and crack growth criteria.

Mots clés: Module de puissance ; Propagation de fissure; Méthode Elements Finis (FEM) Simulations; MOSFET; cycles actifs de puissance; Al métallisation; thermomécanique; CTOD ; durée de vie.

Keywords: Power module; Crack growth; Finite-Elements-Methods (FEM) Simulations; MOSFET; power cycling; chip-metallization; thermomechanics; CTOD; lifetime model.

1 Introduction

In standard power module, the chip-metallization is a thin film of alloyed aluminum deposited onto the silicon substrate, forming bondable metal layer to establish electrical connections with the chip or with other chips via bond wires. Until now 2 different degradation phenomena have been encountered during power cycling: reconstruction and ratcheting.

The reconstruction of the aluminum metallization was encountered in the early years of microelectronics [1], but has begun to be studied only recently [2, 3]. The Al reconstruction is one of the most frequent failure mechanisms observed to affect mainly power modules, with bond wire lift off and solder fatigue [4]. The root cause for Al reconstruction is the Coefficient of Thermal Expansion (CTE) mismatch between Si of chip (2ppm/K) and Al of metallization (25ppm/K). This CTE mismatch is responsible for the generation of high compressive stress within the Al metallization during pulsed operation. This stress is likely to exceed by large the elastic limit. Under these circumstances, the stress relaxation can occur by grain boundary sliding, or by plastic deformation through dislocation glide, depending on temperature and stress conditions [5]. Depending on the texture of the metallization, this leads either to the extrusion of the Al grains or to cavitation effects at the grain boundaries. A large amount of these plastic deformations leads to layer degradation with a subsequent open circuit. Reconstruction is more severe at the center of the chip, as the junction temperature reaches its maximum [3].

Microscopically, the degradation of an Al layer sputtered on Si without any heat treatment, is characterized by 2 phenomena happening in parallel [6]: intergranular cracking and grain size reduction. During heating phase, Al is under compression and its atoms emerge from the inner film through grain boundary and oxidize rapidly. They are forming hillocks. During cooling, the Al layer turns tensile and this causes grain boundary grooving, that is again stabilized by oxidation of bared Al surfaces. Repeating this grooving process leads to intergranular cracking with oxidized boundaries. The division of initially large Al columnar grains may be attributed to regular dislocation processes. Dislocations move easily at relatively low temperature in the Al metallization [7]. Repeated cycles are then prone to accumulate dislocations in the Al grains and therefore create cells that will transform into grains when the added misorientations are sufficient. This classic recovery process is helped by mixed dislocation and diffusion processes such as dislocation climb. The degradation of the Al layer is thus a combined effect of accelerated diffusion at grain boundaries and grains size division by dislocation- based plasticity.

Another mechanism has been shown to induce Al extrusion: the ratcheting [8,9,10]. This ratcheting mechanism occurs because of the CTE mismatch between the Si (2 ppm/K) and the molding compound (~11 ppm/K). At high temperature, the CTE mismatch between mold and Si causes an in-plane compression in Al which goes beyond the elastic limit and therefore induces a plastic flow of the Al. Conversely, at low temperature, the CTE mismatch causes an in-plane tensile strain in Al followed by a plastic strain of the Al when the yield stress is reached. In addition, a constant shear stress, usually due to packaging, is acting on top of the Al, always into the same direction: from the edge to the middle of the chip [11,12]. Independently from the temperature excursion, it gives rise to a shear flow or tilting of the metal every time the yield stress is reached. Consequently, each temperature cycle gives rise to a tilting in the direction to the middle of the chip, which, for many cycles, sums up to considerable amounts. This phenomenon is called ratcheting [13]. At the end, the Al film is not able to transfer the shear stress to the adjacent layers anymore, similarly to a viscous fluid. This can be observed by a wrinkling of the Al metallization.

In this paper, failure mechanisms occurring in an Al metallization of a new power module are investigated. This module is molded and does not have Al wire bonds but a copper clip as

interconnect. This results in a more complicated internal structure than in standard modules and impedes the Al reconstruction or ratcheting. Indeed, here the surface of the Al metallization is not free, but recovered by a solder layer and a Cu clip on its top and surrounded by the molding compound. This new design leads to different failure mechanisms that have to be characterized. Thus, this work aimed at a better understanding of the thermo-mechanical behavior of the metallization layer in this new designed module under Active Power Cycling (APC) with varying load parameters by means of experiments and simulations. This allows the determination of the lifetime of this new module.

2 Design of power module

The power module used in this study is a package made of 6 newly designed MOSFETs. Indeed, those MOSFETs have an electric connection achieved by a copper clip soldered on top of the chip instead of using wire bond (**Erreur ! Source du renvoi introuvable.**a). This structure is more reliable because it avoids wire bond fatigue failures, often the root cause for the device failure. The inner structure of this MOSFET is a bit more complicated than the one of standard power modules. It has some additional material layers on top of the others between the chip and the copper clip (**Erreur ! Source du renvoi introuvable.**1b).

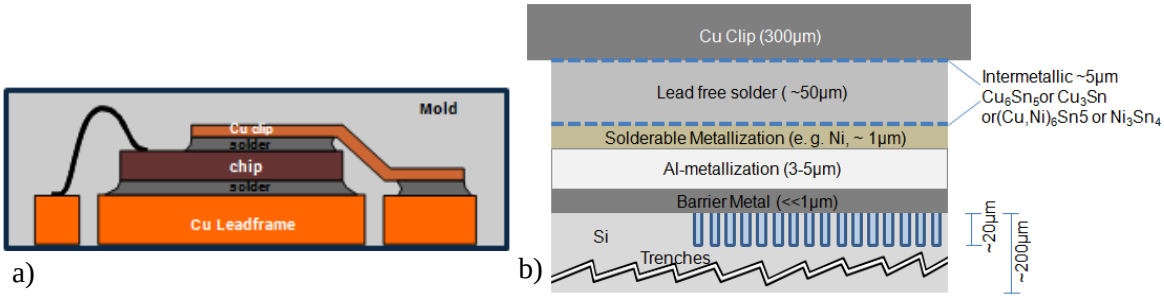

Figure 1: a) Inner structure of a MOSFET with a copper clip and b) scheme of layers composition between the chip and the copper clip of a MOSFET

3 Experimental and numerical methodologies

3.1 Experiments

Active Power Cycling (APC) is the most important reliability test for power modules as it reproduces real working conditions. This test was performed on power modules with copper clips, and only one MOSFET of the package was electrically loaded. The device under test is mounted onto a water-cooled heat sink through the intermediary of a thermal film used as a Thermal Interface Material (TIM). Usually the load current is conducted by the power chip and the power losses heat up the package. Here, the heating current has opposite polarity and is conducted by the body diode of the MOSFET. When the maximum target temperature within the diode is reached, the load current is switched off and the system cools down to a minimum temperature. The end of the cycle is achieved when the minimal temperature is reached. The next cycle begins by starting the load current again. The characteristic parameters for Active Power Cycling tests are: the minimum junction Temperature T_{jmin}, the temperature swing ΔT_j (given by the temperature difference between maximal junction temperature at the end of the heating phase and the minimal junction temperature at the end of the

cooling interval) and the power on-time t_{on}. For power cycling the parameters are typically ranging as follow:

- Current pulse, I_{load}: from 200A up to 600A
- Temperature swing, ΔT_j : from 60K to 130K
- Minimum junction temperature, T_{jmin}: from 20°C to 90°C
- Power on-time (or pulse width), $t_{on:}$ from 0.2s to 60s

About 30 samples were tested with varying test parameters. The current intensity as well as the duration of heating and cooling phase are determined at the beginning of the test and remain constant during the test. The test strategy used here consists in submitting the device to a loading current corresponding to a desired temperature swing ΔT_j and then to repeat the cycle with constant pulse width t_{on} and t_{off}. So the temperature swing is defined at the start, but may vary with ageing effects of the device. This strategy is the most severe method but the closest one to application.

During power cycling, the forward voltage V_f of the body diode and the junction's temperature swing ΔT_j are monitored as they are good indicators of modules health. Indeed, both parameters are likely to increase with ageing effects. T_j is measured via V_f which is a Thermo-Sensitive Parameter (TSP): a measuring current of 10 mA flows through the diode, the V_f is measured and converted into the corresponding T_j through the linear relation existing between both parameter $V_f = f(T_j)$. No fixed End-of-Life criterion was defined, as more knowledge is required on the fatigue resistance of this new designed module. Thus tests were stopped arbitrcarily when the increase of forward voltage V_f or temperature swing ΔT_j was judged high enough.

Before starting the test and at the end of it, power modules are electrically and thermally characterized by measuring leak currents, the resistance R_{DSon} and the thermal impedance Z_{th}. The goal is to evaluate the healthiness of modules after cycling. Metallographic specimens of tested modules were carried out and defects investigated into.

3.2 Simulations

A 2D Finite Element Model (FEM) has been created for a MOSFET with an axisymmetry condition (Figure 2). Such a simplified model of the power package is possible because MOSFETs included in the package are thermally decoupled, meaning that every MOSFET acts as a single one. Moreover, this 2D axisymmetric model with chip-midpoint as symmetry axis provides reliable and precise results. Indeed, the electrical current flows through the center of the chip, thus the chip-midpoint corresponds to the neutral point in terms of thermal expansion.

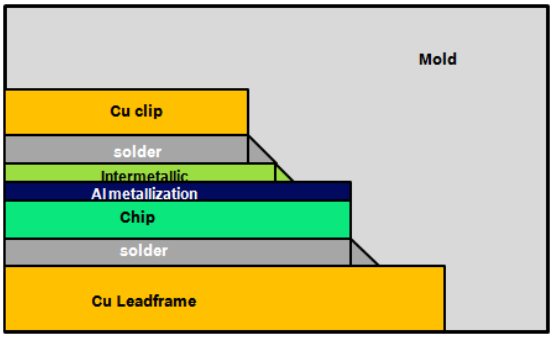

Figure 2: Schematic 2D section of the power device used for simulation

In this FEM model, a fine mesh is defined using quadratic plane elements with 8 nodes. The thinnest layers have a minimum of 4 elements in their thickness, which means that the smallest elements have a size of about 1 µm. Attention was also paid to refine the mesh in the most critical areas of the

module (Figure 3). Both solder layers have fine elements with an aspect ratio of 2.8 and critical areas of the metallization and the intermetallic layer have elements with an aspect ratio of 6.5, which guarantee reliable results. Some elements have a bigger aspect ratio, up to 35, but these elements are not located in critical areas and thus did neither affect the convergence nor results.

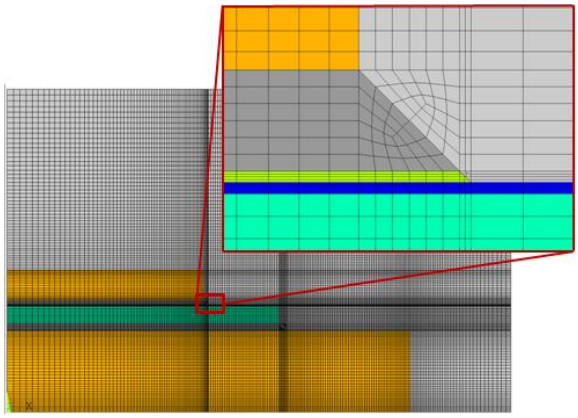

Figure 3: Global view of the mesh with a zoom at a critical area

Thermo-mechanical analysis is performed, which means that thermal results of the transient thermal simulation are imported as loads in the thermo-mechanical simulation. In the thermal analysis, the module is mounted onto a heat sink of aluminum with a constant temperature assumed at its bottom line. Free convection and radiation coming from the air are also taking place on the exterior surfaces of the module. During Active Power Cycling, the chip generates heat which is then dissipated in the entire module. In the mechanical analysis, the power module is not subjected to any pure mechanical loads, the module is only fixed at one point and loads are thermally induced. Three cycles are simulated after an initial cooling down from the stress free temperature of the module to the ambient temperature (Figure 4).

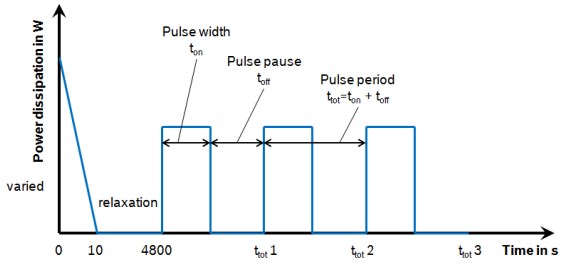

Figure 4: Schematic of the three cycles simulated

The elasto-plastic properties of the copper of the lead frame and the clip were characterized and modeled by a bilinear kinematic hardening. To describe the solder behavior a Garofalo model which defines the secondary creep rate as a function of stress and temperature with a hyperbolic sine was chosen. The SnAgCu solder alloy used was characterized by [14], as follow:

$$\dot{\varepsilon}_{cr} = C_1[sinh(C_2\sigma)]^{C_3} e^{C_4/T} \qquad Eq.\ 1$$

Where $\dot{\varepsilon}_{cr}$ is the steady-state creep strain rate, T the temperature (K), σ the von Mises stress in MPa, and C_1 through C_4 are constants defined as follow in Table 1:

Constant C1 (1/s)	Constant C2 (1/MPa)	Constant C3 (-)	Constant C4 (K)
277984	0.02447	6.41	6500

Table 1: Table of values for the constants of the Garofalo creep law for the SAC solder alloy

The brittle silicon of the chip has linear elastic properties. The chip-metallization is made with an AlCu alloy containing 0.1 % up to 1% Cu. No measurements could have been performed to determine its behavior, but a literature study on the mechanical properties of ~99wt% Al alloys (Al, AlSi, AlCu, AlSiCu) thin film on Si substrate was performed. According to the thickness of our metallization a model with temperature dependent properties was chosen. This model was inspired by [9] and uses a bilinear kinematic hardening to describe the elasto-plastic behavior of the metallization (**Erreur ! Source du renvoi introuvable.**). A literature study was also done for the properties of the intermetallics. They were considered to be pure Cu_6Sn_5 and have a linear elastic model.

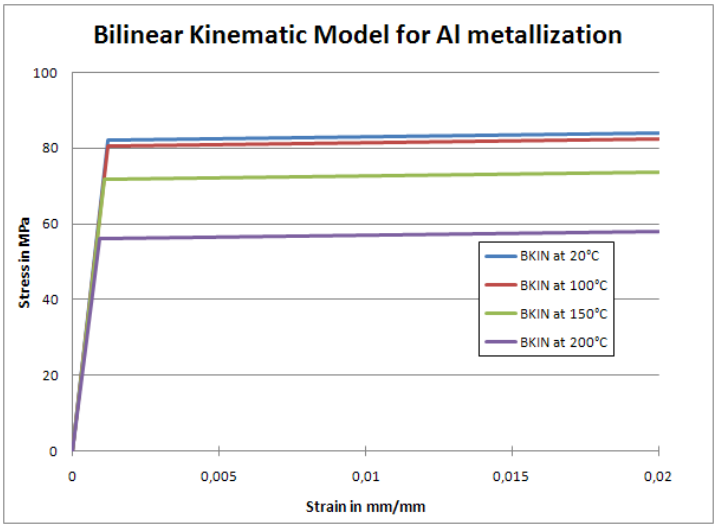

Figure 5: Bilinear kinematic hardening of Aluminum

The commercially available epoxy-based molding compound is a polymer, and has thus a viscoelastic behavior. The material is restricted to be thermorheologically simple. It master curve was implemented through the use of Prony series and the shift operation was defined with the Williams-Landel-Ferry (WLF) shift function (Figure 66).

In the Prony series, the shear modulus is defined as follow:

$$G(t) = G_\infty + \sum_{i=1}^{N} G_i \, e^{-t/\tau_i} \qquad \textit{Eq. 2}$$

Where G(t) is the shear modulus at time t, G_∞ is the long term modulus once the material is totally relaxed, and τ_i are the relaxation times.

The Williams-Landel-Ferry shift function is an empirical equation:

$$\log(a_T) = \frac{-C_1(T - T_r)}{C_2 + (T - T_r)} \qquad \textit{Eq. 3}$$

Where T is the temperature, T_r is a reference temperature chosen to construct the master curve, and C_1 and C_2 are empirical constants adjusted to fit the values of the superposition parameter a_T.

During the assembly process, just after the encapsulation, a post mold cure process takes place. It consists in exposing the module to elevated temperatures, in general 175°C, to speed up the curing process and expedites the cross-linking process of the polymer's molecules. Thus in order to take into account residual stresses due to post mold cure, the stress-free temperature of mold is assumed to be higher (195°C), than the one of the other materials (175°C).

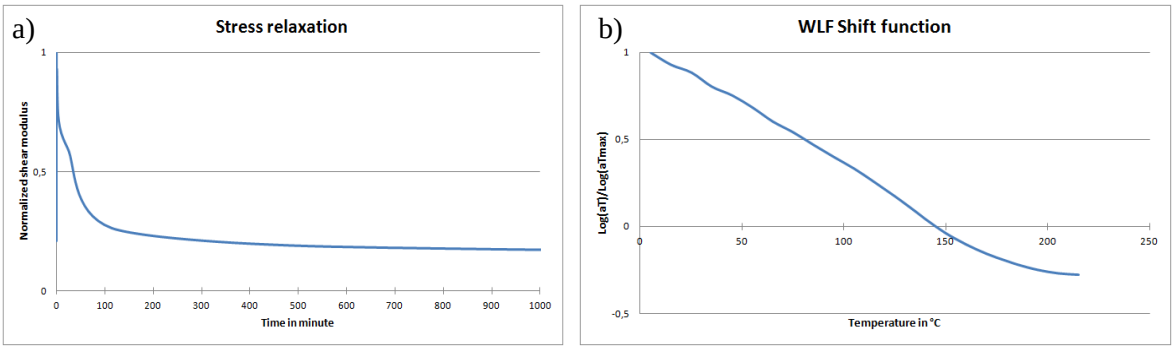

Figure 6: a) Master curve for stress relaxation and b) shift function of the molding compound

With the thermo-mechanical simulation, evolutions of stress and strain in the Al metallization are monitored during power pulses. A study of the sensitivity of various test parameters (minimum junction temperature T_{jmin}, temperature swing ΔT_j, and pulse width t_{on}) is also simulated and the influence of those parameters on the mechanical behavior of power metallization is quantified.
Additionally a fracture mechanic study was performed on the 2D axisymmetric FEM with a crack included in the middle of the thickness of the Al metallization layer. The crack starts under the top solder meniscus and propagates through Al to the center of the module. This crack has a fixed length of 150 µm and was defined using contact and target elements with a friction coefficient to prevent material penetration. Here simulations were performed with varying coefficients of friction and results were not found to be dependent on this value. Thus, the coefficient of friction was arbitrary fixed to 0.2. As the main focus of this study is the crack growth, the global mesh of the module is coarser than in the FEM without cracks. On the other hand, the mesh is refined at the crack tip. In this area, elements are square with a length of about 0.83 µm (Figure 7**Erreur ! Source du renvoi introuvable.**). In the model, the delamination between the molding compound and solder meniscus, which appears after some power cycles, is also taken into account.

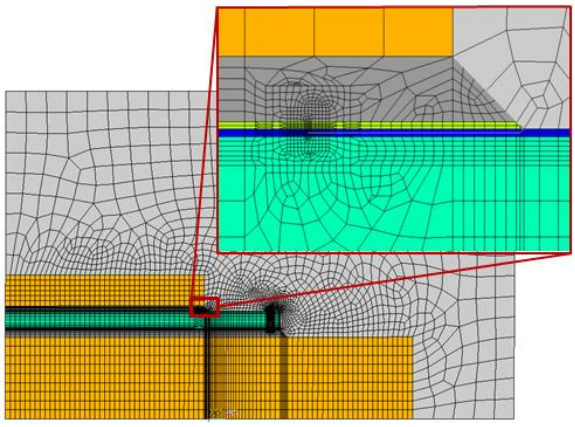

Figure 7: Global view of the mesh with a zoom at the crack tip area

To interpret the crack growth a fracture mechanical criterion was defined. As the Al is an elastoplastic material, a criterion supporting non linear material properties was required. Thus, only the J-integral, the Crack Tip Opening Displacement (CTOD) and the cohesive zone element methods were applicable. The criterion should also work for cyclic loading and has to be compatible with an axisymmetrical model. The J-integral and the cohesive zone element methods are not fulfilling these requirements, as they are not working for cyclic loading and are only defined for plane stress or plane strain conditions. On the other hand, the CTOD criterion allows cyclic loading and axisymmetric conditions. Thus, a mixed mode fracture criterion using the CTOD at a fixed distance behind the crack tip as the fracture parameter was manually implemented. The CTOD criterion [16] states that crack growth occurs when the current CTOD reaches a critical value and the direction of crack growth is the direction that leads to the maximum opening or shearing CTOD component value at the new crack tip. For this study the critical value of the CTOD is not known, but the crack growth will probably be subcritical and it is still interesting to see the influence of the various test parameters from the sensitivity study on the evolution of the CTOD component value.

4 Degradations of the Al metallization under APC

Some Active Power Cycling tests were performed on MOSFETs with different experimental parameters: T_{jmin} ranges from -30°C to 60°C, ΔT_j varies from 60K to 120K and t_{on} ranges from 0.2s to 10s. Some representative cases were taken out of the 30 tests performed and are presented in the Table 2 in order to have a general idea on tests and results in terms of Al degradations.

T_{jmin}	-30°C				15°C						45°C ≤ Tjmin ≤ 70°C		
ΔT_j	60K	120 K			60 K	90 K	120K				60K	90 K	110K
t_{on}	0,2s	0,5s	2s	5s	0,2s	0,5s	0,2s	0,5s	2s	10s	0,2s	0,2s	0,35s
t_{off}	0,8s	2,5s	7s	10s	3s	4,5s	3,8s	3,5s	6s	5s	1,2s	2,8s	1,15s
Number of cycles	3 000 000	510 000	110 000	220 000	1 000 000	830 000	428 000	1 430 000	911 000	262 983	2 270 000	2 068 510	629 543
increase in Vf	-	+3,5%	+1%	+6%	-	+0,5%	+6,2%	+6,5%	+6%	+25%	+1%	-	+6,6%
increase in ΔT	-	+17%	+3,5%	+12,5%	-	-	+13,5%	+8,3%	+8%	+40%	-	-	+22%
increase in Z_{th} between 2e-4s and 0,02s	-	yes	yes	-	-	-	yes	-	yes	problem	-	yes	yes
increase in R_{dson}	+6,5%	+62%	+29%	+193%	-9%	+0%	+45%	+43%	+20%	problem	+15,5%	+23%	+54%
Degradation in Al	-	deformation, long cracks, and migration at top solder meniscus	delamination Al/top solder at top solder meniscus	deformation delamination Al/ top solder and migration at top solder meniscus	-	strong degradation and cracks at top solder meniscus	deformation, delamination Al/ top solder, cracks and migration at top solder meniscus	big deformation under the dimple area, delamination Al/top solder, cracks and migration at top solder meniscus	slight deformation and long cracks at top solder meniscus	deformation and cracks at top solder meniscus	-	delamination and cracks at top solder meniscus	strong deformation and migration at top solder meniscus
crack length max in Al (µm)	-	1279	-	-	-	-	-	904	929	-	-	1055	-
% delaminated surface top solder/AlCu	-	44,44	60	-	-	-	-	80	20	-	-	21,74	73,33

Table 2: Recap chart of 13 of the 30 APC tests performed with the resulting Al degradations

Tests were stopped arbitrarily when an important increase in the body diode forward voltage V_f or in the temperature swing ΔT_j was noticed. There was no fixed End-of-Life criterion defined for this module at this stage of the study. Tests were stopped usually after 100.000 to 2 million cycles, and modules were always electrically functional at the end of tests. This proves the high reliability of such power modules with double sided soldered chips. Despite this very good endurance, modules are submitted to degradation phenomena. Metallographic specimens of tested devices were prepared and defects investigated into using optical microscope and Reflection Electron Microscope (REM). Different types of degradation in Al were highlighted (Figure 8): deformation of the layer (a), migration of Al in the top solder (b**Erreur ! Source du renvoi introuvable.**), delamination between Al and top solder (c), and cracks within the layer (d). Those degradations appear at the area of Al located under the top solder meniscus. Cracks and delamination between top solder and Al often

start at this solder meniscus area, and then propagate to the center of the MOSFET. This differs from standard modules, where reconstruction occurs preferably at the center of the chip and wrinkles due to ratcheting develop from the edge to the middle of the chip.
Degradations of the Al metallization were sometimes accompanied by a slight increase in thermal impedance Z_{th} at the beginning of the measurement. This can be explained by the fact that a degraded Al metallization affects the top side cooling path of the module, which represents 5% of the total cooling of the MOSFET and evacuates the heat from the chip, through the metallization, the top solder the Cu clip and the mold to the air.

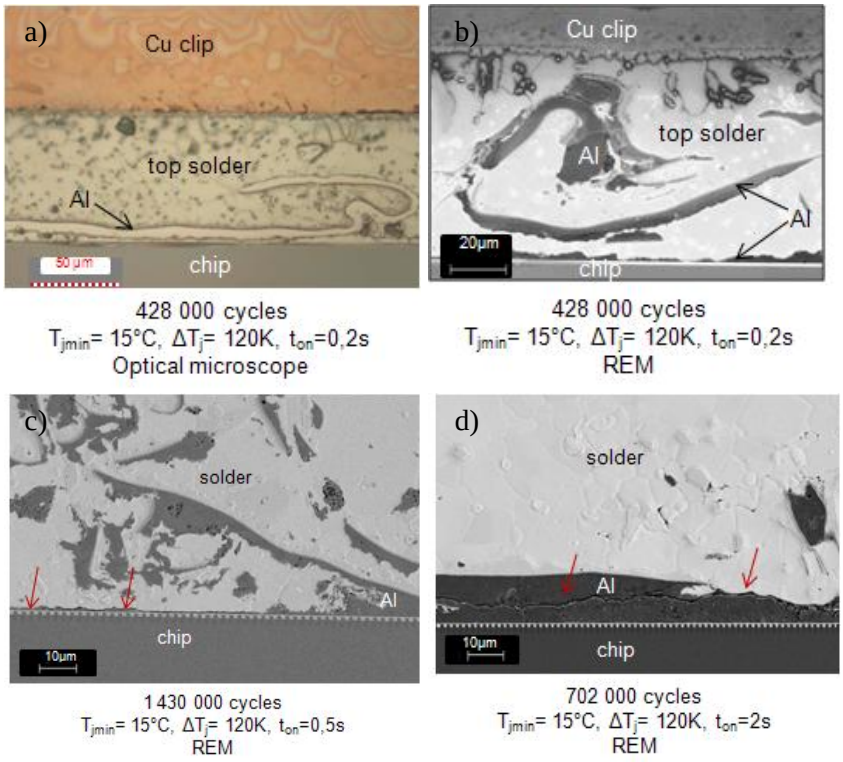

Figure 8: Images of a) a strong Al deformation, b) migration of Al in the top solder, c) delamination at the interface Al/ top solder and d) a crack inside the Al metallization

By looking at the table, it appears that the presence of degradations in the Al metallization is almost always accompanied by a significant increase in R_{DSon}. This originates from the fact that a degraded Al disturbs the distribution of current to the chip. Moreover cracks and deformations in Al are reported for all cases except for tests performed with $\Delta T_j = 60K$ and stopped after several million of cycles. So increasing the temperature swing ΔT_j seemed to accelerate the degradation of the Al layer. From these experimental results, it can be concluded that the Al metallization degradation is a systematical failure mechanism leading to the degradation of the electrical behavior of the module.

5 Lifetime prediction

As the Al metallization degradation is a main failure mechanism in our module, an End-of-Life (EoL) criterion could be based on the R_{DSon} increase. The definition of an EoL criterion is important and would allow us to compare tests results in function of the different tests parameters. Until now, the only EoL criterion available is used for standard IGBT module and defines the EoL by an increase in V_{ce} of 5% (corresponding to an increase in 1% in V_f for our module) as it usually corresponds to a wire

lift-off. As our module does not have wire bonds but a Cu clip, this criterion does not correspond to a specific failure mechanism occurring in the module and thus may be too severe. For example, some devices which had reached an increase in V_f greater than 1% were still electrically functional and did not show critical degradations inside the package.
On the Figure 9a is plotted the percentage of degraded area in the Al metallization in function of the increase in R_{DSon}. A trend line emerges out of the results, thus a correlation exists between the percentage of area degraded in the Al metallization and the increase in R_{DSon}. This confirms that an appropriate EoL criterion for our module can be defined based on the R_{DSon} increase. Moreover, it means that we have now a non destructive method to determine the amount of degradations in the module, simply by measuring the R_{DSon}. But as the R_{DSon} increase was not continuously monitored, another relation as to be found between a parameter continuously monitored during the test (V_f or ΔT_j) and the increase in R_{DSon} in order to be able to determine the new EoL criterion.

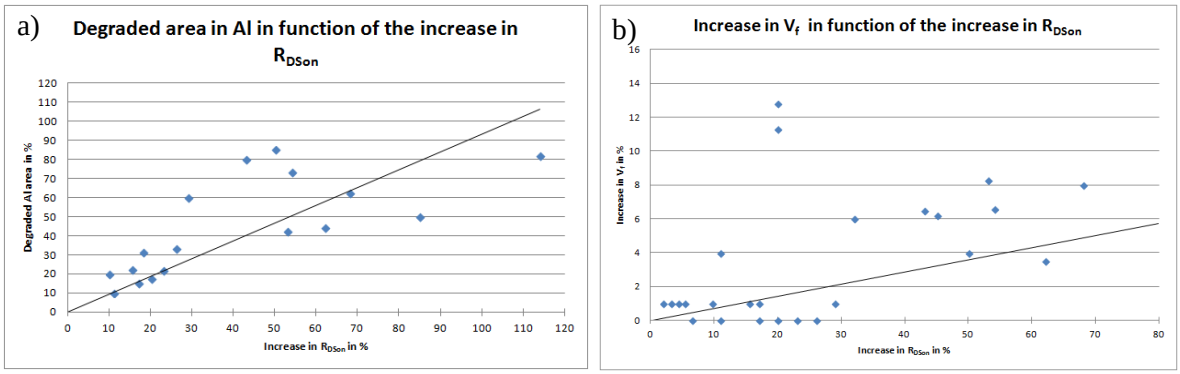

Figure 9: a) Percentage of degraded area in the Al metallization versus the increase in R_{DSon} and b) the increase in V_f versus the increase in R_{DSon}

The increase in V_f in function of the increase in R_{DSon} is plotted **Erreur ! Source du renvoi introuvable.**9b. Results are quite scattered, thus the correlation between the increase in V_f and R_{DSon} is not really good. The poor quality of this correlation suggests that an optimization of our test method could be to regularly measure the R_{DSon} in good thermal conditions during the tests. Thus the R_{DSon} could be directly used to define an EoL criterion. Despite the poor quality of the correlation between the increase in R_{DSon} and V_f, this one will still be used to define a new EoL criterion.

In a first approach an acceptable limit of degradation in our module is a degraded area of 40% in the Al metallization. Indeed, tested modules which had such a degraded area in the Al were still electrically functional. This 40% of degraded area is correlated to an increase in R_{DSon} of about 40% (Figure 9), itself correlated to an increase of 3% in V_f (**Erreur ! Source du renvoi introuvable.**). So a first suggestion for a more appropriate EoL criterion could be an increase in V_f of 3%. A better adjusted EoL criterion can certainly be found by performing some more experiments and by regularly measuring the R_{DSon}. But this is already a first step in the determination of an appropriate EoL criterion for our module. The lifetime of modules tested was calculated based on the new EoL criterion and is plotted and compared to the lifetime based on the standard EoL criterion in function of ΔT_j (Figure 10). Fewer results are obtained for the lifetime based on the new criterion as for some samples the test was stopped before that an increase in V_f of 3% was observed. But this already gives an idea of the gain of lifetime with the new EoL criterion. And the gain of lifetime is non negligible as changing from an EoL criterion of an increase in V_f of 1% to an increase of 3% already double the lifetime prediction of the module.

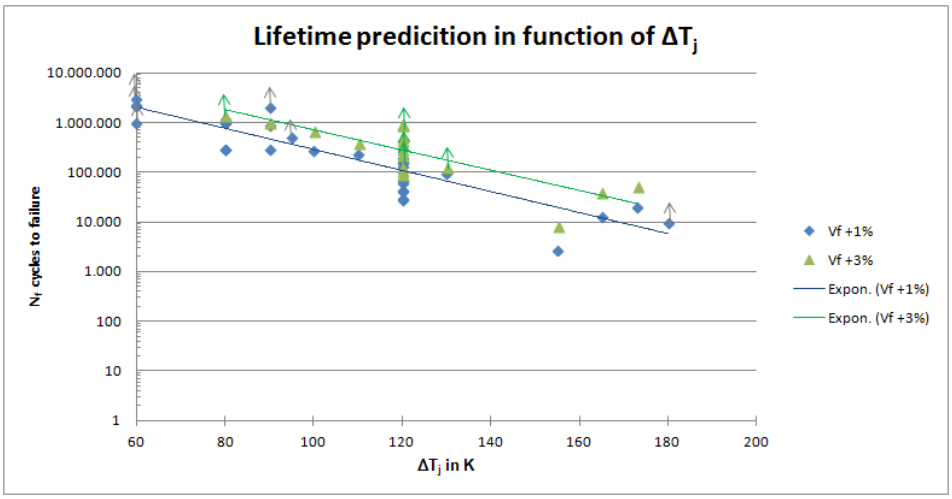

Figure 10: N_f cycles to failure in function of ΔT_j with EoL V_f +3% and EoL V_f +1%

6 Simulation results

A path was defined in the middle of the Al metallization, from its center to one of its extremity, to be able to observe the evolution of stresses and plastic strain in function of the position in Al. One simulation case (T_{jmin}= -40°C, ΔT_j=120K, t_{on}= 10s) is taken as a representative example to describe mechanisms that are taking place in the metallization layer. The different stresses were analyzed [17] and it was found that the "in-plane" stress drives the von Mises stress and that at high temperatures, Al is under compressive stress, whereas at low temperatures tensile stress is dominant.

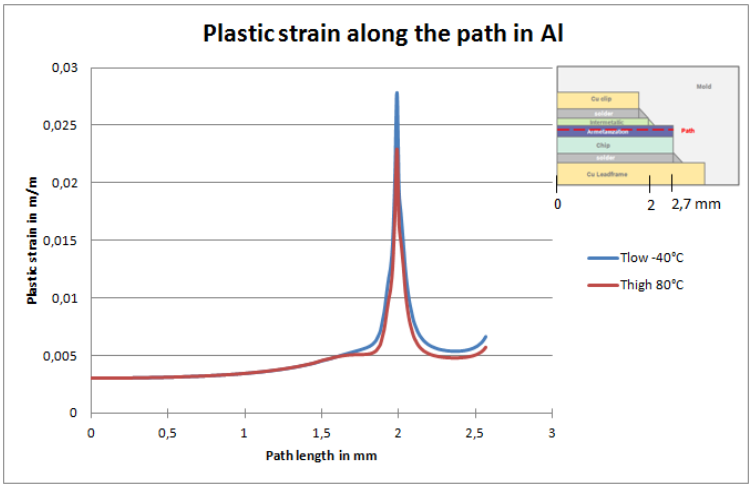

Figure 11: Plastic strain along a path in Al for the case T_{jmin}= -40°C, ΔT_j=120K, t_{on}= 10s

Now the plastic strain curves is plotted along the path at different times of the pulse period (Figure 11) and the importance of the zone under the top solder meniscus is highlighted as a peak of plastic strain is observed exactly at this position**Erreur ! Source du renvoi introuvable.**. In order to better understand the mechanisms Al is submitted to in this critical area, it is interesting to analyze the correlation between the evolution of the temperature, the accumulated plastic strain and the von Mises stress during one cycle. Therefore, the accumulated plastic strain per cycle was calculated by averaging the plastic strain obtained along the path in the area beneath the top solder meniscus, and was then plotted together with the evolution of temperature and von Mises stress (Figure 12**Erreur !**

Source du renvoi introuvable.). More precisely, the plastic strain average was calculated for the values obtained between 1.983mm to 1.993mm along the path in the Al. At the beginning of the temperature pulse, the von Mises stress originates from the initial conditions: a 175°C stress free temperature is defined and the module is cooled down to room temperature. This gives the frozen internal stresses within the package. Now, when the system heats up, these inner stresses decrease and reach a minimum value. By continuing the heating up process, the stress changes its direction and the von Mises stress and the plastic strain increase simultaneously. Then the temperature remains constant, and a stress relaxation without an increase in the plastic strain can be observed. The stress relaxes under constant plastic strain because of the solder layer on top of the Al metallization, which transfers its stress relaxation behavior. In the following cooling phase the same behavior is repeated, with the opposite deformation direction. The accumulated plastic strain follows the temperature changes and increases by heating up or cooling down, and stays constant at constant temperature. One can also notice that the accumulated plastic strain is higher during the cooling phase than during the heating phase.

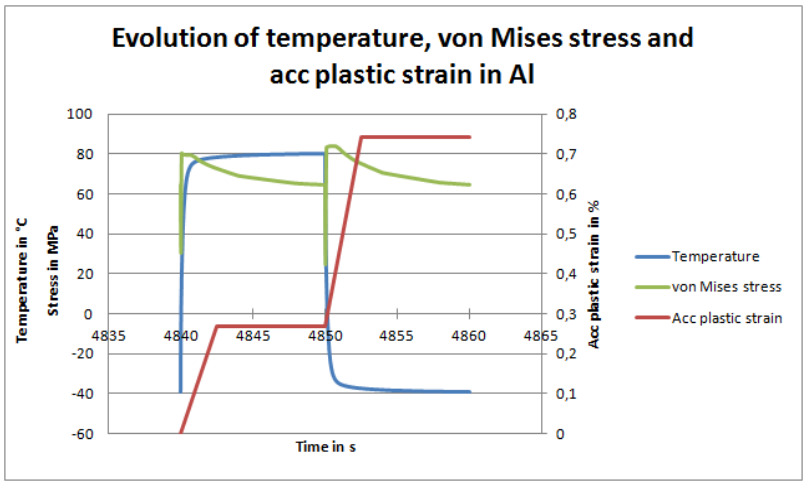

Figure 12: Evolution of temperature, von Mises stress and accumulated plastic strain in Al at the critical area beneath the top solder meniscus during 1 cycle for the case T_{jmin}= -40°C, ΔT_j=120K, t_{on}= 10s

Then, results of the fracture mechanical simulation are analyzed. First of all, the crack zone shows a large scale yielding. Then, in order to have a better understanding of crack growth in Al, the evolution of the CTOD criterion in function of time has to be plotted for both opening mode (Figure 13) and "in plane" shear mode (Figure 14). For the opening mode, a negative displacement represents a crack closing and a positive displacement represents a crack opening. At high temperatures the crack is closed while at low temperatures the crack is open. The crack opening remains narrow as the maximum displacement observed is under 0.01 µm. This may be explained by the fact that the Cu clip soldered on top of the Al metallization and the mold are restricting out of plane displacements and thus crack opening. A slight shift in the maximum and minimum displacement values is noticeable with an increasing number of cycles for both opening and shearing mode. This shift comes from the rate dependent properties of the top solder. The CTOD needs a few more cycles to stabilize, but its amplitude stays constant. As the study do not focus on the evolution of displacement's extremums but on the amplitude of displacement, calculating 3 cycles is sufficient for our analysis.

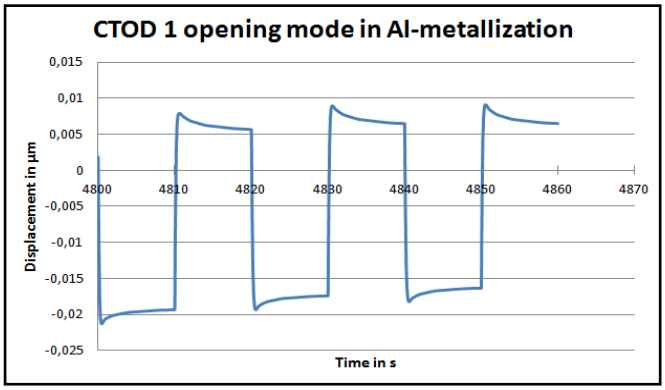

Figure 13: Evolution of the CTOD criterion for the opening mode in function of time for the case T_{jmin}= -40°C, ΔT_j=120K, t_{on}= 10s

For the shear mode, a negative CTOD represents a displacement to the left and a positive CTOD represents a displacement to the right for the layer above the crack compared to the layer underneath. In this case, the layer above the crack is always shifted to the left in comparison to the layer underneath. At low temperatures, the layer above the crack is moving further to the left, and at high temperatures, the layer above the crack is coming back to the right. Shear displacements are quite important as the maximal CTOD value reached is about 0.4 µm. This means that the maximum shearing component of CTOD is 40 times higher than the maximum opening component. So the absolute maximum value of CTOD component at the new crack tip is obtained by the shearing component, and thus crack growth will occur along a local mode 2 direction.

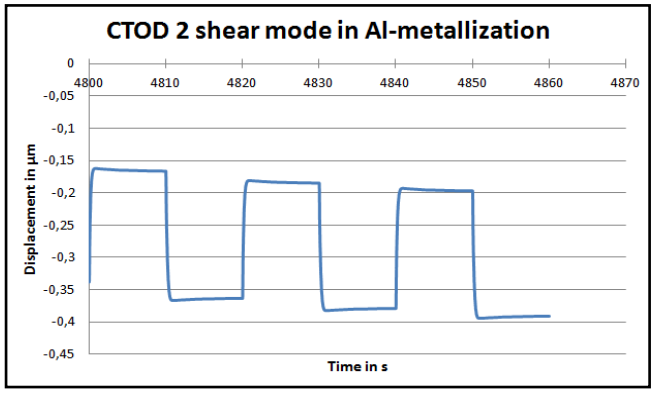

Figure 14: Evolution of the CTOD criterion for the "in plane" shear mode in function of time for the case T_{jmin}= -40°C, ΔT_j=120K, t_{on}= 10s

7 Sensitivity study

A sensitivity study of tests parameters (T_{jmin}, ΔT_j, and t_{on}) was simulated and the influence of those parameters on accumulated plastic strain and CTOD component is quantified. With both experiments and simulations, it was pointed out that there is a critical region in the chip metallization: the area located just beneath the top solder meniscus. The accumulated plastic strain in this zone for one cycle was calculated and plotted for different sets of parameters (Figure 15). The influence of test parameters on plastic strain is quite clear. First of all, the lower T_{jmin} is, the higher the percentage of plastic strain will be. Then, high temperature swings are needed for the accumulation of plastic strain in one cycle.

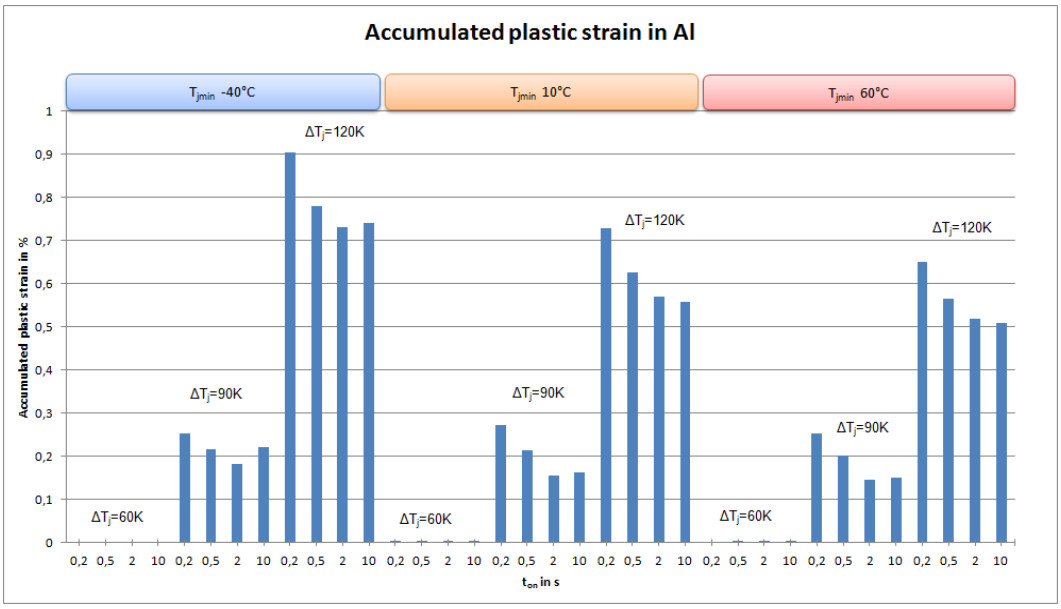

Figure 15: Histogram of accumulated plastic strain in Al in 1 cycle for different sets of test parameters

For small temperature swings like ΔT_j=60K which corresponds to field load, there is no accumulated plastic strain. This correspond with what was already observed in experiments, as several modules did not shown any degradations in Al after several million of power cycles with ΔT_j=60K. This raises the question to know if the same failure mechanisms are taking place under ΔT_j=60K and under ΔT_j=90K or 120K. By looking more closely at the histogram, it is noticeable that for ΔT_j=60K, there is no accumulated plastic strain at all with T_{jmin} = -40°C and really small amount of accumulated plastic strain of about $1e^{-6}$ with T_{jmin} = 10°C and 60°C. Thus, for the Al metallization it is not exactly the same failure mechanism occurring under ΔT_j=60K and ΔT_j =90K or 120K, as there is no plastic deformations for ΔT_j=60K. Finally, short pulses also generate more accumulation of plastic strains in Al. Indeed, power pulses lead to spatially inhomogeneous temperature distribution in the module. With short pulses, the spatial temperature gradient is even more important inside the module, thus generating more Al plastic deformation. Consequently, low start temperatures with large temperature swings and short pulses are the most critical tests parameters in terms of plastic metallization deformation.

For both opening and shearing component of CTOD (Figure 16 and Figure 17), 3 values are to be taken into account: the minimum and maximum value of CTOD component reached in one cycle, and the amplitude of CTOD variation which is the difference between the maximal and minimal values of the CTOD component. The amplitude is of main interest, and the minimum and maximum allow understanding in which direction the crack is moving. For mode 1 (Figure 16), at high temperatures, displacements are minimal, so the crack is closed. At low temperatures, displacements are maximal and the crack is open. Looking at the histogram, one can notice that all minimal and some maximal values of CTOD for mode 1 are negative. Those negative values depend on the definition of contact stiffness in simulations and thus don't have a real physical meaning. That is why the interpretation of those results is still in question. Despite that fact, it is possible to identify some main trends regarding the influence of test parameters on the crack opening mode. In terms of crack opening amplitude in Al: low T_{jmin} with large temperature swings ΔT_j are the most critical parameters. The pulse width t_{on} does not seem to have a big influence on the crack opening amplitude. Results of shearing mode are also influenced by the closed crack situation, as the closed contact with friction coefficient has effects on stress distribution.

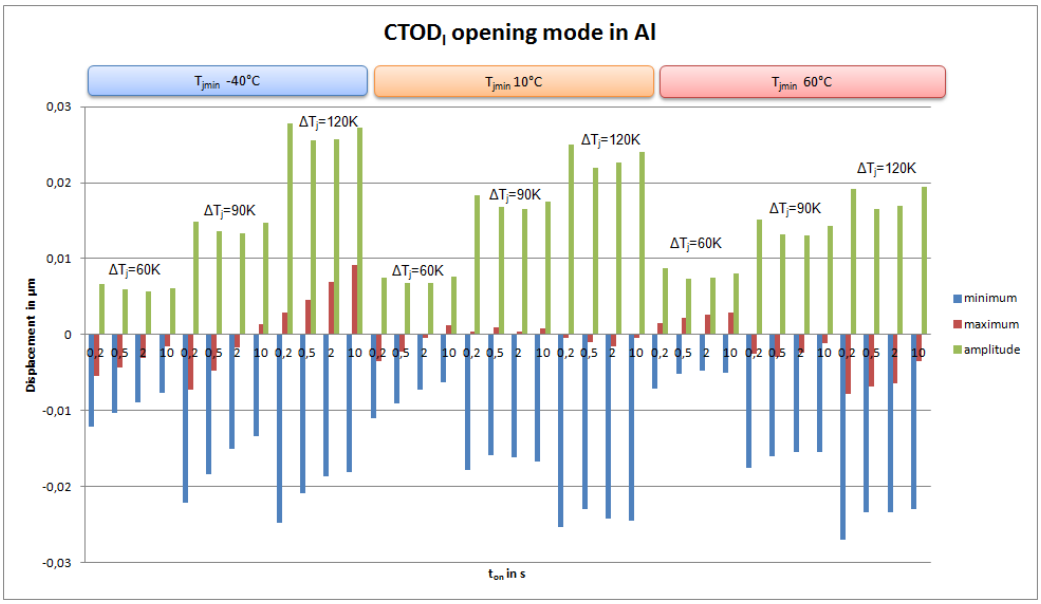

Figure 16: Histogram of opening component of CTOD in 1 cycle for different sets of test parameters

For mode 2 (Figure 17), at high temperatures, the CTOD reaches it absolute minimum, meaning that the layer above the crack is moving to the right side. At low temperatures, the CTOD reaches it absolute maximum, so the layer above the crack is moving to the left side. First, one notices that the amplitude of displacement for mode 2 follows the same trend as for mode 1. Thus, to summarize: low T_{jmin} with large temperature swings ΔT_j are the most critical parameters in terms of shearing amplitude for the crack in Al. The influence of the pulse width t_{on} on the shearing amplitude of crack is difficult to determine.

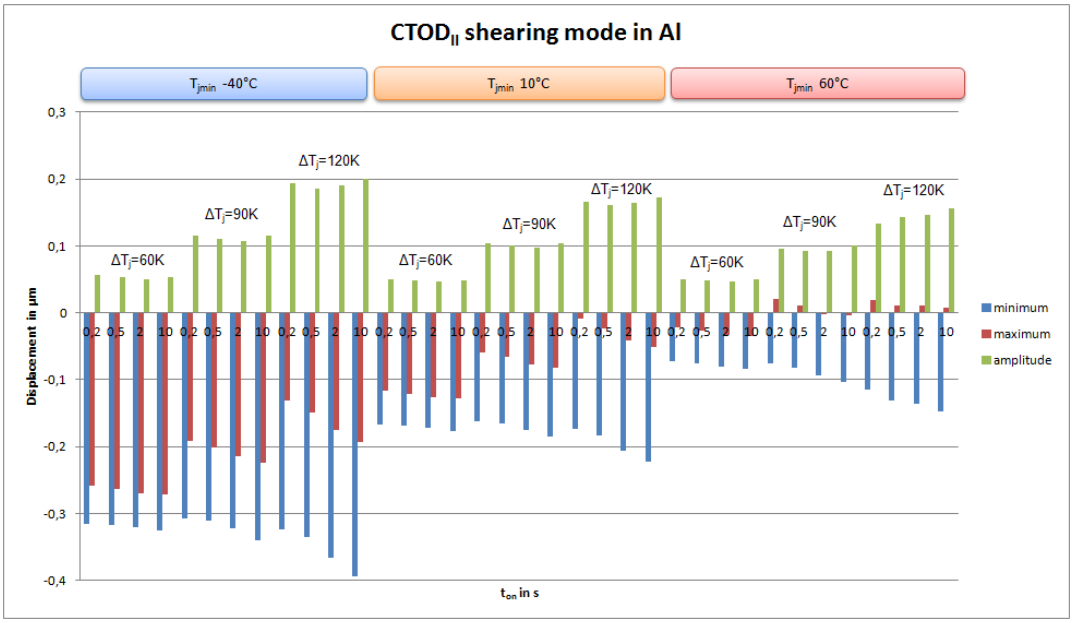

Figure 17: Histogram of shearing component of CTOD in 1 cycle for different sets of test parameters

Comparing values of CTOD's components for mode 1 and mode 2, it is noticeable that shearing displacements are clearly dominant (approximately 10 time higher than opening displacements) for all loading cases of the sensitivity study. This large predominance of shearing CTOD component

compared to the opening one, added to the difficulties to properly interpret results for opening CTOD component, lead us to conclude that the shearing mode is the most critical one and therefore the only one to be taken into account.

Based on experiments it can also be deduced that the crack growth probably remains subcritical as no catastrophic failures were observed even after high number of cycles. Then, the **Erreur ! Source du renvoi introuvable.** presents the worst set of test parameters (T_{jmin}, ΔT_j and t_{on}) for each output parameter analyzed (plastic strain and both CTODs) for Al metallization. It appears that large ΔT_j with low T_{jmin} are critical for plastic deformation and crack growth. The only difference is concerning the power on-time t_{on}. For plastic strain, short pulses are critical, whereas for both CTODs, t_{on} does not seem to have a significant influence.

	Inputs			
Outputs	of output parameters	T_{jmin}	ΔT_j	t_{on}
	Acc plastic Al	↘	↗	↘
	$CTOD_1$ Al	↘	↗	=
	$CTOD_2$ Al	↘	↗	=

Table 3: Recap chart of the worst sets of parameters regarding plastic deformations and crack propagation in the Al metallization

8 Lifetime models

With the experimental APC tests, a lifetime prediction in function of different sets of test parameters was obtained. With the FEM simulations, amounts of plastic strains and CTODs, also called output parameters, were calculated for different sets of test parameters. Combining the results obtained from both experiments and simulations, allow plotting a lifetime prediction correlating the experimentally obtained lifetime with the corresponding calculated plastic strain and CTODs… Then a power trend line fitting the best the scattered points was determined. The trend line equation defines then the lifetime model in the form of a Coffin Manson model:

$$N_f = a \cdot (x)^{-b} \qquad \textit{Eq. 4}$$

Where N_f is the number of cycles to failure, a a coefficient and b an exponent determined with experiments and x the output parameter.

Then regarding the lifetime requirements under APC, these ones are strongly dependent on the application of the module. However it can be roughly consider that with ΔT_j= 80-90K, a lifetime of 100 000 cycles is a minimum required while a lifetime of 1 million of cycles characterized already a robust module.

First the lifetime is predicted in function of the acc plastic strain in the Al metallization Figure Erreur **! Il n'y a pas de texte répondant à ce style dans ce document.**18. Some tests were stopped before reaching the EoL, hence a lack of reliability observed for the trend lines. The values of acc plastic strain are ranging from 0.13% to 2.2%, and the lifetime decreases quite rapidly in this interval. For the lowest amount of acc plastic strain, a lifetime of 2.4 million of cycles is reached, and for the highest amount of acc plastic strain the lifetime is divided by 45 and attains only 53 500 cycles. This lifetime of 53 500 cycles is quite short and was obtained by testing under ΔT_j=170K.

The Coffin Manson lifetime model deduced has the form:

$$N_f = 164309 \cdot (\varepsilon_{acc\ pl})^{-1.317} \qquad Eq.5$$

With $\varepsilon_{acc\ pl}$ the acc plastic strain in the Al metallization.

Thus in order to have a lifetime equal or superior to 500 000 cycles, the acc plastic strain has to stay equal or inferior to 0.43%. Thus 0.43% of acc plastic strain could define a critical limit for the Al metallization lifetime.

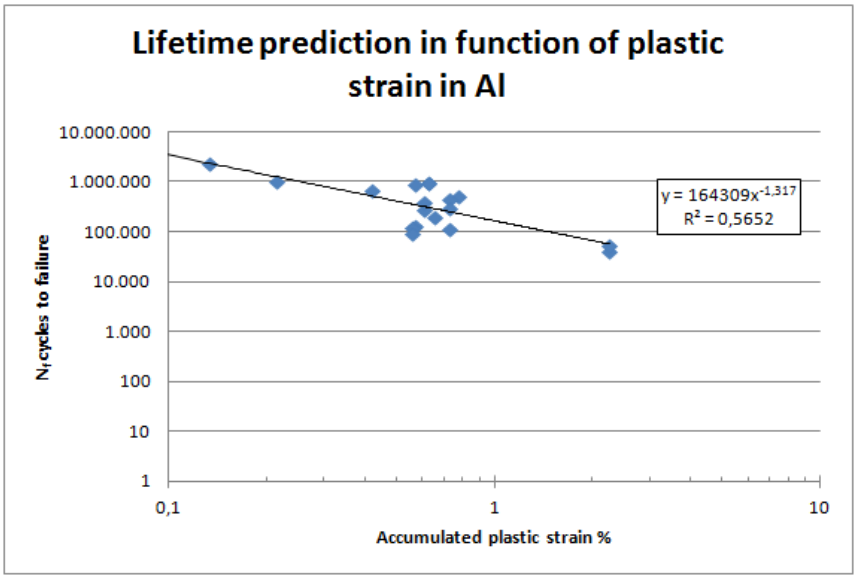

Figure ***Erreur ! Il n'y a pas de texte répondant à ce style dans ce document.****18: N_f cycles to failure in function of the acc plastic strain in the Al metallization*

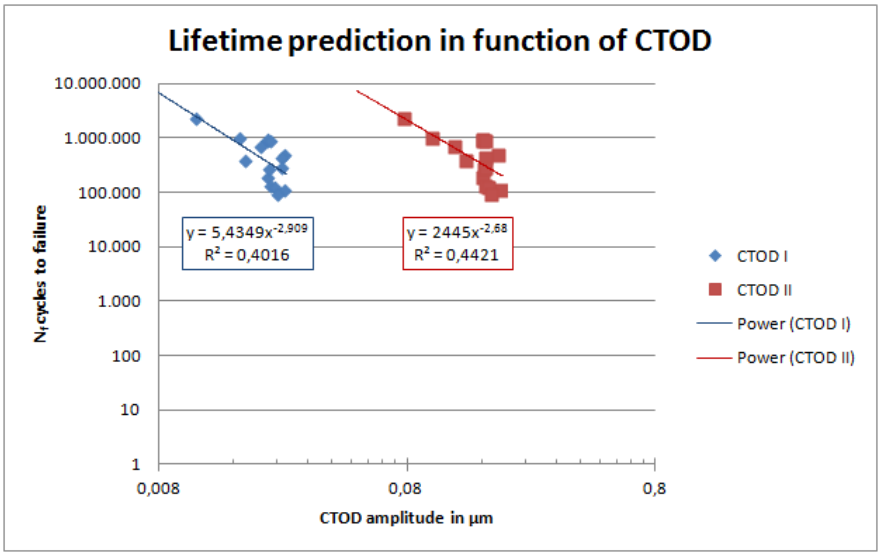

Figure 19: N_f cycles to failure in function of the $CTOD_I$ and $CTOD_{II}$ amplitudes in the Al metallization

Concerning the crack growth in the Al metallization, the lifetime is predicted in function of both $CTOD_I$ and $CTOD_{II}$ amplitudes Figure 19. For both $CTOD_I$ and $CTOD_{II}$, their trend lines are only moderately reliable. Then it appears clearly on the graphic that the opening mode generates smaller amplitude of displacements than the shearing mode. Trend lines of both CTOD have similar profile

with a quite rapid lifetime decrease with increasing amplitude of CTOD, but still do not have the same slope and equation.
With a $CTOD_I$ amplitude of 0.011µm a lifetime of 2.4 million of cycles can be reached, whereas a $CTOD_I$ amplitude about 2 times higher, of 0.025 µm induces a lifetime approximately divided by 5, with 450 000 cycles. These results are describing a very reliable module, as the worst case described was reached under ΔT_j=120K and has a lifetime already close to 500 000 cycles.
Regarding results of the mode II, with a $CTOD_{II}$ amplitude of 0.08 µm a lifetime of 2.4 million of cycles can be reached, and a $CTOD_{II}$ amplitude 2 times higher (0.16 µm), divides the lifetime by 8, with 292 000 cycles. Here also results are really good, as the worst case described was reached under ΔT_j=120K and still has a lifetime already above 100 000 cycles. The Coffin Manson lifetime model deduced has the form:

$$N_f = 2445 \cdot (\Delta CTOD_{II})^{-2.68} \qquad Eq.6$$

With $\Delta CTOD_{II}$ the amplitude of $CTOD_{II}$ at the crack tip in the Al metallization.
Thus in order to have a lifetime equal or superior to 500 000 cycles, the amplitude of $CTOD_{II}$ has to stay equal or inferior to 0.14 µm. Thus 0.14 µm of $CTOD_{II}$ amplitude could define a critical limit for the Al metallization lifetime.

9 Conclusion

After power cycling, deformations and cracks in the chip-metallization of a new designed MOSFET module are found to appear in the area beneath the top solder meniscus. These degradations in Al metallization are found to correlate with an increase in the R_{DSon} of the MOSFET. This allows the definition of an appropriate EoL criterion for our module. This criterion states that the EoL is reached when the R_{DSon} has increased of 40%, which corresponds to 40% of degraded area in the Al metallization. Thanks to this EoL definition, the influence of the test parameters on the module's lifetime can be analyzed.
Finite Elements simulation, confirms that the area beneath the top solder meniscus is critical, as a peak of plastic strain occurs exactly at this location. Based on the evaluation of plastic deformation at the critical area, a numerical sensitivity study on tests parameters is conducted. Low T_{jmin} with large temperature swings ΔT_j and short pulses t_{on} are the most critical test parameters. It was also determined that it is actually not the same failure mechanism occurring under field loads ΔT_j=60K and under accelerated tests with ΔT_j=90K or 120K. Indeed, for small temperature swings ΔT_j corresponding to field loads, no plastic deformations of Al occurs neither in simulation nor in experiments. Thus, it is actually not possible to accelerate the failure mechanism of the Al metallization.
Then, crack growth is numerically investigated with the help of a mixed mode fracture criterion based on Crack Tip Opening Displacement. There is opening and shearing of the crack at low temperatures, whereas at high ones, the crack is closed. So, as expected, low T_{jmin} with large temperature swings ΔT_j are the most critical test parameters for both opening and shearing criteria. The pulse width t_{on} does not seem to have a significant influence on crack propagation. The clear predominance of shear mode must be noted, thus indicating that the Al crack growth occurs along a local mode 2 direction.
Finally lifetime models were deduced by correlating the experimentally obtained lifetime with the corresponding calculated plastic strains and CTODs. The lifetime models deduced from this study could be further improved by carrying out more experiments with an improved test stand. Indeed, in order to improve the EoL criterion of the module, the R_{DSon} should be regularly measured during the APC tests and in adequate thermal conditions.

References

[1] C. Santoro, Thermal cycling and surface reconstruction in aluminum thin films, Journal of the Electrochemical Society, Vol. 116, No. 3, (1969), pp. 361–364

[2] P. Malberti, M. Ciappa, R. Cattomio, A power-cycling induced failure mechanism of IGBT multichip modules, Int. Symposium for Testing and Failure Analysis, (1995), Vol. 21, pp. 163–168

[3] M. Ciappa, and P. Malberti, Plastic Strain of Aluminum Interconnections during Pulsed Operation of IGBT Multichip Modules, Quality and Reliability Engineering International, Vol. 12, (1996), pp.297-303

[4] M. Ciappa, Selected Failure Mechanisms of Modern Power Modules, Microelectronics Reliability, Vol. 42, (2002), pp. 653-667

[5] G.P. Zhang, C.A. Volkert, R. Schwaiger, R. Mönig, and O. Kraft, Fatigue and Thermal Fatigue Damage Analysis of Thin Metal Film, Microelectronics Reliability, Vol. 47, No. 12, (2007), pp. 2147–2151

[6] D. Martineau, T. Mazeaud, M. Legros, Ph. Dupuy, and C. Levade, Characterization of Alterations on Power MOSFET Devices under Extreme Electro-thermal Fatigue, Microelectronics Reliability, Vol. 50, (2010), pp. 1768-1772

[7] M. Legros, M. Cabie, and D.S. Gianola, In-situ Deformation of Thin Films on Substrate, Microscopy Research and Technique, Vol. 72, No.3, (2009), pp. 270-283

[8] W. Kanert, Reliability Challenges for Power Devices under Active Cycling, 47th Annual International Reliability Physics Symposium, (2009)

[9] W. Kanert, R. Pufall, O. Wittler, R. Dudek, and M. Bouazza, Modelling of Metal Degradation in Power Devices under Active Cycling Conditions, 12th Int. Conf. on Thermal, Mechanical and Multiphysics Simulation and Experiments in Microelectronics and Microsystems, EurosimE, (2011)

[10] T. Smorodin, J. Wilde, P. Alpern, and M. Stecher, A Temperature-Gradient-Induced Failure Mechanism in Metallization under Fast Thermal Cycling, IEEE Trans-Device and Materials Reliability, Vol. 8, No. 3, (2008), pp.590–599

[11] Z. Suo, Reliability of Interconnect Structures, Comprehensive Structural Integrity, Vol. 8, Elsevier, Amsterdam, (2003), pp.265–324

[12] M. Huang, Z. Suo, Q. Ma, and H. Fujimoto, Thin Film Cracking and Ratcheting caused by Temperature Cycling, Journal of Materials Research, Vol. 15, No. 6, (2000), pp. 1239-1242

[13] M. Huang, Z. Suo, and Q. Ma, Plastic Ratcheting Induced Cracks in Thin Film Structures, Journal of the Mechanical and Physics of Solids, Vol. 50, (2002), pp. 1079-1098

[14] A. Schubert, R. Dudek, E. Auerswald, A. Gollhardt, B. Michel, and H. Reichl, Fatigue Life Models for SnAgCu and SnPb Solder Joints Evaluated by Experiments and Simulations, Electronic Components and Technology Conf., (2003), pp. 603-610

[15] H.A Richard, Bruchvorhersagen bei überlagerter normal- und schubbeanspruchung von rissen, VDI Forschungsheft 631, VDI-Verlag, Düsseldorf, (1985), pp. 1-60

[16] F. Ma, X. Deng, M.A Sutton, and J.C Jr. Newman, A CTOD-Based Mixed-Mode Fracture Criterion, Mixed-Mode Crack Behavior, ASTM STP 1359, American Society for Testing and Materials, West Conshohoken, PA, 1999, pp. 86-110

[17] C. Durand, M. Klingler, D. Coutellier, and H. Naceur, Study of Fatigue Failure in Al-Chip-Metallization under Power cycling, Engineering Fracture Mechanics, Vol.138, (2015), pp.127-145